Geostatistical simulation of two-dimensional fields of raindrop size distributions at the meso-γ scale

M. A. Schleiss,[1] A. Berne,[1] and R. Uijlenhoet[2]

Received 23 October 2008; revised 6 April 2009; accepted 1 May 2009; published 18 July 2009.

[1] The large variability of the raindrop size distribution (DSD) in space and time must be taken into account to improve remote sensing of precipitation. The ability to simulate a large number of 2-D fields of DSDs sharing the same statistical properties provides a very useful simulation framework that nicely complements experimental approaches based on DSD ground measurements. These simulations can be used to investigate radar beam propagation through rain and to evaluate different radar retrieval techniques. The proposed approach uses geostatistical methods to provide structural analysis and stochastic simulation of DSD fields. First, the DSD is assumed to follow a Gamma distribution with three parameters. As a consequence, 2-D fields of DSDs can be described as a multivariate random function. The parameters are normalized using a Gaussian anamorphosis and simulated by taking advantage of fast Gaussian simulation algorithms. Variograms are used to characterize the spatial structure of the DSD fields. The generated fields have identical spatial structure and are consistent with the observations. Because intermittency cannot be simulated using this technique, the size of the simulation domain is limited to the meso-γ scale (2-20 km). To assess the proposed approach, the method is applied to data collected during intense Mediterranean rainfall. Taylor's hypothesis is invoked to convert time series into 1-D range profiles. The anisotropy of the fields is derived from radar measurements. Simulated and measured reflectivity fields are in good agreement with respect to the mean, the standard deviation, and the spatial structure, demonstrating the promising potential of the proposed stochastic model of DSD fields.

Citation: Schleiss, M. A., A. Berne, and R. Uijlenhoet (2009), Geostatistical simulation of two-dimensional fields of raindrop size distributions at the meso-γ scale, *Water Resour. Res.*, *45*, W07415, doi:10.1029/2008WR007545.

1. Introduction

[2] Because of the complex interactions between atmospheric dynamics and cloud microphysics, precipitation is highly variable over a large range of space and time scales [e.g., *Berndtsson and Niemczynowicz*, 1988; *Groisman and Easterling*, 1994; *Xie and Arkin*, 1997]. This variability is a significant source of uncertainty for the measurement, the simulation and the forecasting of precipitation as well as of the environmental processes influenced by it. For example, the variability of land surface hydrology is strongly controlled by the variability of precipitation [*Syed et al.*, 2004].

[3] To investigate aspects of the large space-time variability of precipitation, a simulation approach is able to provide known reference data from which a variety of sources of uncertainty can be studied quantitatively. Hence a lot of attention has been devoted to the development of techniques to simulate 2-D or 3-D precipitation fields [*Foufoula-Georgiou and Krajewski*, 1995; *Pegram and Clothier*, 2001]. These techniques can be divided in two main categories: (1) physical approaches that aim at simulating the physical processes involved in precipitation (e.g., ARPSO [*Xue et al.*, 2000]) and (2) statistical approaches that consider precipitation as a random variable in space and time. Within the latter category, different techniques have been applied: point processes and clustering [e.g., *Waymire et al.*, 1984; *Onof et al.*, 2000], self-similarity [e.g., *Gupta and Waymire*, 1993; *Menabde et al.*, 1997], and geostatistics [e.g., *Guillot*, 1999; *Bouvier et al.*, 2003]. The proposed methods focus solely on the simulation of rain rate values.

[4] Remote sensors do not directly measure the rain rate but rather some observables which are related to the electromagnetic properties of the ensemble of drops within the considered sampling volume. In the case of weather radars, the conversion of radar reflectivity values into rain rate values is strongly influenced by the microstructure of rainfall (mainly by the size, the shape and the fall velocity of individual raindrops). The fall velocity and the shape of raindrops are closely related to their equivolumetric diameter [*Beard*, 1976; *Andsager et al.*, 1999]. Therefore the raindrop size distribution (DSD) is of critical importance for the quantitative interpretation of radar measurements. Similarly to rain rates, the DSD is highly variable in space and time [*Tokay and Short*, 1996; *Jameson and Kostinski*, 2001; *Uijlenhoet et al.*, 2003]. This variability must be taken into account to improve radar rain rate estimates.

[5] To analyze the different sources of uncertainty in radar rain rate estimates using a simulation approach, it is

[1] Laboratoire de Télédétection Environnementale, École Polytechnique Fédérale de Lausanne, Lausanne, Switzerland.
[2] Hydrology and Quantitative Water Management, Wageningen University, Wageningen, Netherlands.

0043-1397/09/2008WR007545$09.00

necessary to include information about the spatial variability of the DSD. Simulation methods based on point processes have been developed [e.g., *Lavergnat and Golé*, 2006] but so far cannot provide 2-D or 3-D fields of DSDs. Conditional simulation methods have also been proposed. Starting from simulated rain rate fields, [*Krajewski et al.*, 1993] derived a consistent Gamma DSD assuming uniform and uncorrelated distributions of the DSD parameters. These are strong assumptions, not supported by the data used in this paper. More recently, *Lee et al.* [2007] proposed to use measured radar reflectivity fields in combination with ground-based DSD measurements to generate DSD fields. In this case, the highest spatial resolution is imposed by the radar resolution, which is usually of the order of 1 km^2. Hence this approach does not allow to investigate the radar subgrid variability of the DSD. Simulations of correlated DSD fields based on point DSD measurements do not have this limitation. However, to date such techniques have only been proposed to simulate time series or 1-D range profiles [*Berne and Uijlenhoet*, 2005; *Montopoli et al.*, 2008].

[6] The main objective of this paper is to develop a stochastic simulation framework allowing for conditional as well as nonconditional simulation of 2-D fields of DSDs using point DSD measurements. Geostatistics provides useful tools for the analysis and the simulation of random fields with complex spatial structures [*Chilés and Delfiner*, 1999; *Lantuéjoul*, 2002]. The ability to generate a large number of statistically homogeneous fields can be used to obtain reliable statistical characterizations of a variety of issues related to radar beam propagation through rain as well as radar retrieval techniques. It is worth mentioning that such a simulation framework may also be useful for other domains dealing with the propagation of radio waves in the atmosphere. Satellite or ground-based microwave communication is a relevant illustration [*Dissanayake et al.*, 1997; *Fong et al.*, 2003].

[7] The paper is organized as follows: section 2 describes the modeling of the DSD. The simulation framework is detailed in section 3. The simulator is applied and evaluated using data collected during an intense Mediterranean rain event in section 4. Finally, the conclusions and perspectives are given in section 5.

2. Modeling the DSD

2.1. Gamma Model

[8] The DSD describes the number of drops per unit volume and per unit size interval of equivolumetric spherical drop diameter. It is supposed to be adequately described by a Gamma distribution [*Ulbrich*, 1983; *Willis*, 1984] given by the following expression:

$$N(D) = \alpha N_t D^{\mu} \exp(-\Lambda D), \tag{1}$$

where $N(D)$ (m^{-3} mm^{-1}) denotes the number of drops per unit volume with diameters between D (mm) and $D + dD$ and $\alpha = (\int_{D_{\min}}^{D_{\max}} D^{\mu} e^{-\Lambda D}\, dD)^{-1}$ is a normalization factor taking into account the finite range of possible drop sizes between $D_{\min}$ and $D_{\max}$. The Gamma DSD depends on three parameters: the shape $\mu > -1$ (dimensionless), the rate $\Lambda > 0$ (mm^{-1}) and the concentration $N_t > 0$ (m^{-3}).

2.2. Gaussian Anamorphosis of DSD Parameters

[9] DSD parameters (μ, Λ, N_t) can be interpreted as correlated random functions in space and time with a theoretical multivariate distribution function F. Simulating realistic DSD fields means generating independent realizations of (μ, Λ, N_t) according to F. In theory, this requires the complete knowledge of all the finite dimensional distributions of F, which is rarely the case in practical applications. Furthermore, finding a simulation algorithm for any given distribution function F is known to be a very difficult problem, as pointed out by *Lantuéjoul* [2002].

[10] A possible solution is to transform the original distribution F into a Gaussian distribution for which a variety of simulation algorithms have been developed (e.g., sequential simulation, turning bands, spectral decomposition). Such a transformation is called a Gaussian anamorphosis [*Journel and Huijbregts*, 1978; *Guillot*, 1999]. At the end of the simulation, the inverse transformation is applied to retrieve the original parameters.

[11] For multivariate continuous distributions, a possible Gaussian anamorphosis is given by the stepwise conditional transformation [*Leuangthong and Deutsch*, 2003]. The advantage of stepwise conditional transformation is that it creates independent jointly Gaussian variables that can be simulated separately. The relations between the original variables (e.g., the correlations and higher-order moments) are preserved in the back transformation process.

[12] For n variate problems, the nth variable is transformed conditionally to the first $n - 1$ variables, as follows:

$$Y_n = \Phi^{-1}\left[F_{n|1,\ldots,n-1}(z_n|z_1,\ldots,z_{n-1})\right], \tag{2}$$

where $F_{n|1,\ldots,n-1}$ is the conditional distribution function of the nth component given $z_1,\ldots,z_{n-1}$ and $\Phi$is the cumulative distribution function of a standardized Gaussian random variable. For $n = 1$, this reduces to $Y_1 = \Phi^{-1}[F_1(z_1)]$. If it exists, the inverse transformation is given by $Z_n = F^{-1}_{n|1,\ldots,n-1}[\Phi(y_n)|y_1,\ldots,y_{n-1}]$.

[13] In practical applications where $F_{n|1,\ldots,n-1}$ is unknown, the conditional distributions must be estimated from the sample. This can be done empirically by discretizing the space of parameters or by applying more complex methods [e.g., *Diciccio et al.*, 1993; *Hall et al.*, 1999]. In each case, the inverse transformation is approximated using a correspondence table between the original and the transformed variables, which implies that simulated fields will in the end be composed of measured values only. Inversion problems may arise when many data share the same value. This is unlikely with continuous distributions but may happen for mixed distributions like those produced by intermittent rain fields where the marginal distribution of N_t has an atom at zero. Therefore the presented simulator is limited to nonintermittent rainfall fields, which is a reasonable assumption up to scales of the order of 20 km, also referred as the meso-γ scale [*Orlanski*, 1975].

3. Geostatistical Simulation of DSD Fields

3.1. Modeling the Spatial Structure of DSD Fields

[14] Previous studies have shown that the 3 parameters, μ, Λ and N_t that describe the Gamma DSD model are highly variable in space and time [e.g., *Tokay and Short*, 1996;

Ulbrich and Atlas, 1998]. This must be taken into account for accurate radar rain rate estimation. Because of their variability, μ, Λ and N_t can be seen as realizations of random variables. In theory, rainfall is an intrinsically discrete process consisting of individual drops. Nevertheless, it can be seen as a continuous quantity when considering bulk variables like the rain rate or the radar reflectivity factor integrated over scales larger than a few cubic meters. At these scales, DSD parameters can also be considered continuous in space and time and the values of (μ, Λ, N_t) can be interpreted as realizations of a multivariate random function [*Yaglom*, 2004]. Geostatistics has been developed to provide a mathematical framework for the analysis of such random functions [*Matheron*, 1965].

[15] The fundamental tool for the analysis of the spatial structure of a random function $Z(x)$ is the semivariogram (called variogram in the following):

$$\gamma(h) = \frac{1}{2} E\left[(Z(x+h) - Z(x))^2\right], \tag{3}$$

where E denotes the expectation, $x \in R^2$ is a position vector and $h \in R^2$ is a separation vector. The variogram is only defined if $Z(x)$ is an intrinsic random function, meaning that its increments $Z(x + h) - Z(x)$ must be second-order stationary [*Chilés and Delfiner*, 1999, pp. 16–17]. This assumption, however, is less restrictive than second-order stationarity of the variable $Z(x)$ itself.

[16] If $\gamma(h)$ only depends on the norm of h, the random function is said to be isotropic. In general, however, random functions are anisotropic, meaning that $\gamma(h)$ depends both on the norm of h and on its direction. Finally, a variogram must satisfy some mathematical properties: in particular, $-\gamma(h)$ must be an even, nonnegative positive definite function with $\gamma(0) = 0$ [*Chilés and Delfiner*, 1999, pp. 57–63]. In general, variograms are preferred to covariances for two reasons: (1) they are more general than covariances because they do not assume finite variance of the random function and (2) they do not require any knowledge about the mean of the sample.

[17] In practice, variograms must be estimated from the sample. This can be done by using the following standard expression:

$$\hat{\gamma}(h) = \frac{1}{2N(h)} \sum_{x_k - x_l \sim h} [z(x_k) - z(x_l)]^2, \tag{4}$$

where $N(h)$ represents the number of observations separated by a vector h. This estimate is known to be asymptotically unbiased. However, it is sensitive to the presence of outliers and measurement errors in the sample. Therefore, more robust alternatives to the standard variogram estimate have been proposed [e.g., *Cressie and Hawkins*, 1990].

[18] Note that in general $-\hat{\gamma}(h)$ is not a positive definite function and hence does not verify the mathematical properties of a variogram. Therefore, a common approach is to fit a theoretical model on the sample variogram. Popular variogram models are exponential, spherical or Gaussian functions [*Chilés and Delfiner*, 1999, pp. 80–93]. Several variograms can be combined to create nested structures. In particular, the sum of two variograms (of the same type) is still a valid variogram.

3.2. Simulation of the DSD Fields

[19] This section explains how to generate realistic 2-D fields of DSDs by using the geostatistical tools introduced in section 3.1.

[20] First, the DSD parameters (μ, Λ, N_t) are fitted on measured DSD spectra and normalized using a Gaussian anamorphosis (see section 2.2) to obtain a new set ($\tilde{\mu}, \tilde{\Lambda}, \tilde{N}_t$) of independent and centered parameters. Sample variograms are computed on the transformed parameters and fitted using a theoretical variogram model. A Gaussian simulation algorithm is used to generate independent fields of ($\tilde{\mu}, \tilde{\Lambda}, \tilde{N}_t$) with spatial structure given by the fitted variogram models. At the end of the simulation, the inverse anamorphosis is applied to retrieve the original DSD parameters. Bulk variables characterizing rainfall such as the radar reflectivity factor Z (mm^6 m^{-3}) can be derived from the fields at both horizontal and vertical polarization using the following expression:

$$Z_{H|V} = \frac{10^6 \lambda^4}{\pi^5 |K|^2} \int_{D_{\min}}^{D_{\max}} \sigma_{B_{H|V}}(D) N(D) dD, \tag{5}$$

where $\sigma_{B_{H|V}}(D)$ (cm^2) is the backscattering cross section of a drop with diameter D (mm) at the given polarization, λ (cm) is the wavelength, and K is the dielectric factor of liquid water, a function of the complex relative permittivity.

[21] The simulation method described above can be applied to produce both conditional and nonconditional simulations. Conditional simulations are particular realizations which honor observed values at some specified locations within the considered domain, whereas nonconditional simulations are just independent realizations of the same random function. Since nonconditional simulations can be easily transformed into conditional ones [e.g., *Chilés and Delfiner*, 1999, p. 465], the following application will focus solely on the simulation of nonconditional fields.

4. Application

[22] This section presents an application of the proposed DSD simulator using the statistical software package "R" (http://www.r-project.org) together with the "Gstat" package by *Pebesma* [2004].

4.1. Data

[23] In theory, the description of the spatial and temporal variability of DSD fields requires large data sets of DSD measurements in space and time. As far as the authors know, such data sets are not yet available at a resolution that is sufficient to capture the variability of DSD fields over a large range of scales. Therefore, the following application has been parameterized using time series of DSD measurements instead of spatial measurements. The considered time series was collected on 11 September 1998 during the HIRE'98 experiment that took place in Marseille, southern France (R. Uijlenhoet et al., HYDROMET Integrated Radar Experiment (HIRE): Experimental setup and first results, paper presented at 29th Conference on Radar Meteorology, American Meteorological Society, Montreal, Canada, 1999). A rain event of about 2 h and representative of intense Mediterranean precipitation was simultaneously observed by an optical disdrometer and by an S band

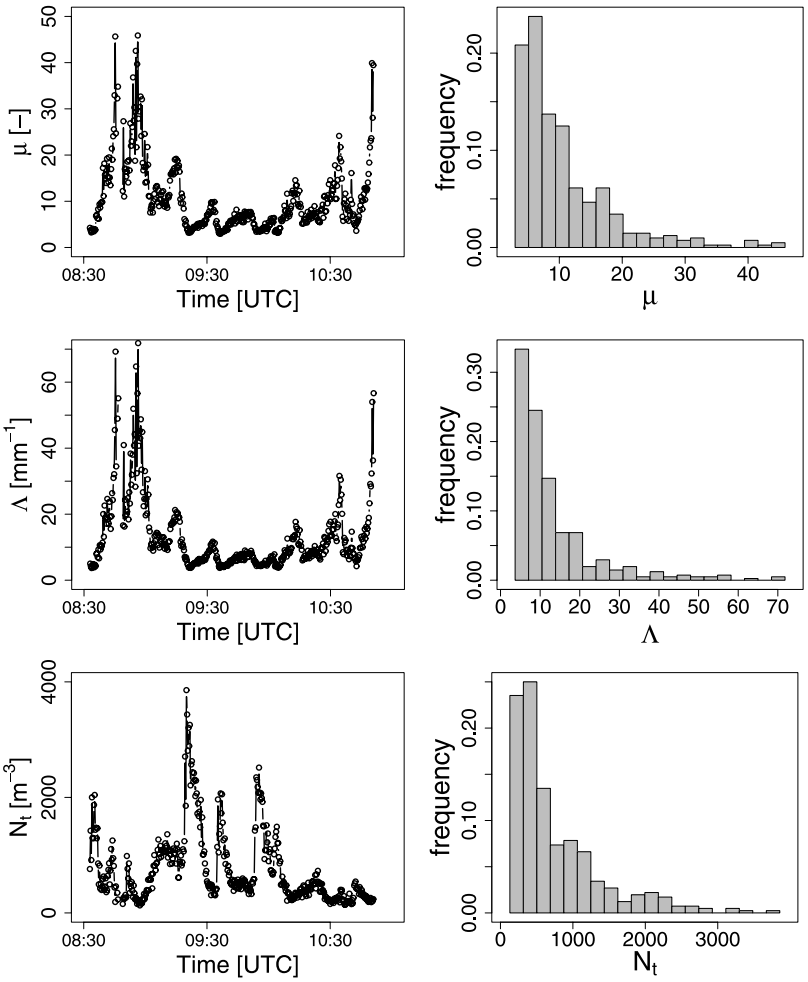

Figure 1. Time series and empirical distributions of the DSD parameters (μ, Λ, N_t) before the anamorphosis.

weather radar (10 cm wavelength) operated by Météo France and located at about 100 km from Marseille. The optical disdrometer was operated at a 20-s time resolution and collected 415 DSD measurements during the event. The total rain amount seen by the disdrometer over the 2 h was 27 mm for a maximum intensity of 80 mm h^{-1}. The choice of the 20-s time resolution is a tradeoff between availability of enough data for the structural analysis and limitation of the sampling effects due to high temporal resolution.

4.2. DSD Fitting

[24] For each of the 415 DSD spectra recorded by the disdrometer, a three-parameter Gamma DSD was fitted using the maximum likelihood method. This method has already been employed in previous investigations including *Haddad et al.* [1997] and *Kliche et al.* [2008]. Maximum likelihood estimators are known to be asymptotically unbiased, efficient and Gaussian distributed [e.g., *van der Vaart*, 1998]. For small samples, however, they must be handled with care since significant uncertainty can be introduced in the estimates [*Uijlenhoet et al.*, 2006]. Figure 1 shows the time series of the fitted DSD parameters together with their empirical marginal distributions. The average number of drops per fit is 242. Only 7 DSD spectra contained less than 30 drops and could not be fitted properly. Note the large correlation (0.99) between and μ and Λ the negative correlation (-0.40) between μ and N_t, respectively, between Λ and N_t (-0.37).

4.3. Gaussian Anamorphosis of DSD Parameters

[25] Clearly, the marginal distributions of the DSD parameters are not Gaussian. Therefore, a Gaussian anamorphosis (see section 2.2) is performed to obtain a new set of independent parameters ($\tilde{\mu}, \tilde{\Lambda}, \tilde{N}_t$) with joint Gaussian distribution. The conditional distributions needed for the transformation are approximated by discretizing the space of parameters into 30 regularly spaced bins. Here we can take advantage of the strong correlation (0.99) between μ and Λ, which makes it particularly easy to estimate their conditional distributions. The number of discretization bins has been chosen after testing several alternative possibilities and is a tradeoff between availability of enough points for the estimation and limitation of the bias. The normality of the joint distribution is confirmed by performing a Mardia

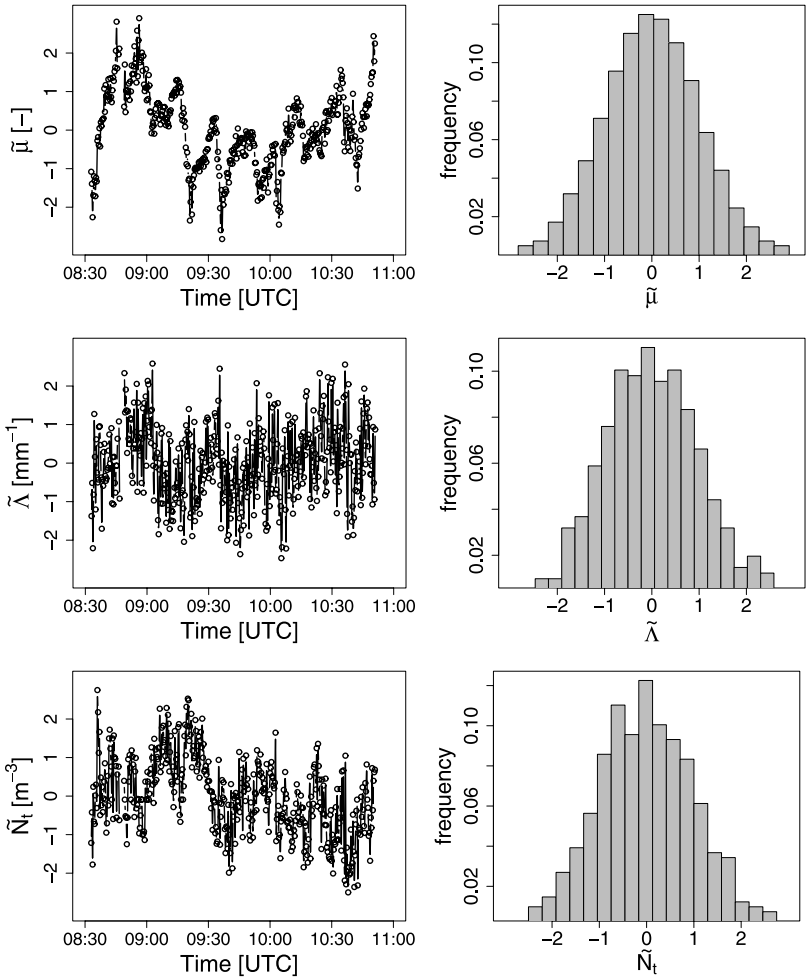

Figure 2. Time series and empirical distributions of the DSD parameters $(\tilde{\mu}, \tilde{\Lambda}, \tilde{N}_t)$ after the anamorphosis.

test [*Mardia*, 1970] and a multivariate version of the Shapiro-Wilk test [*Srivastava and Hui*, 1987]. The independence assumption is confirmed by performing a standard t test on the correlations. Figure 2 shows the transformed DSD parameters together with their empirical marginal distributions. A correspondence table between original and transformed variables is used to approximate the inverse transformation.

4.4. Testing Taylor's Hypothesis

[26] According to *Berne et al.* [2004], the average rainstorm movement velocity during the described event was about 12.5 m s^{-1} in the NE direction (i.e., azimuth of 50°). Time series of $(\tilde{\mu}, \tilde{\Lambda}, \tilde{N}_t)$ can thus be converted into a 1-D range profile along the direction of advection by assuming Taylor's hypothesis of frozen turbulence. The spatial resolution (250 m) of this profile is determined by the time resolution (20 s) and the average advection speed (12.5 m s^{-1}).

[27] Note that Taylor's hypothesis is a strong assumption that is not required by the simulator but necessary in absence of spatial DSD data. Reflectivity measurements taken by the radar can be used to quantify the quality of Taylor's hypothesis. The method consists in shifting the fields in time and space for a given advection speed and direction (in this case 12.5 m s^{-1} and 50° with respect to the North). If the fields result from pure advection by a constant wind, the shifted pixels should overlap on average, meaning that in the (Z, Z_{shift}) space, Taylor's hypothesis is represented by a straight line with slope 1 and intercept 0. The quality of Taylor's hypothesis can thus be verified by looking at the correlation between Z and Z_{shif} and at the ratio of their means. Figure 3 represents these values for

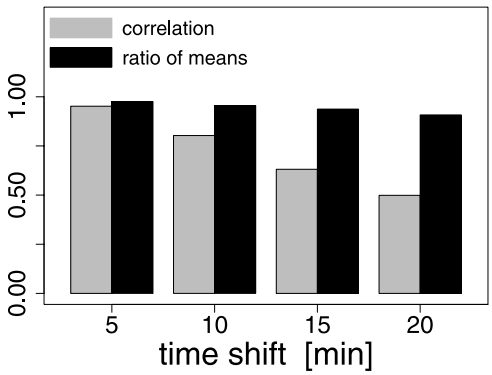

Figure 3. Verification of Taylor's hypothesis for time shifts of 5–20 min. Under the hypothesis of pure advection, both the correlation and the ratio of means should be equal to 1.

Table 1. Nugget, Range, and Partial Sill Values of Two Nested Spherical Models Fitted to the Sample Variograms of $(\tilde{\mu}, \tilde{\Lambda}, \tilde{N}_t)$[a]

	Nugget	Range 1	Partial Sill 1	Range 2	Partial Sill 2
$\tilde{\mu}$	0.03	7	0.63	18	0.26
$\tilde{\Lambda}$	0.67	4	0.25	14	0.04
$\tilde{N}_t$	0.29	3	0.35	12	0.21

[a]All ranges are given in km. The sills for $\tilde{\Lambda}$ and $\tilde{N}_t$ are given in mm^{-2} and m^{-6}, respectively.

time shifts from 5 to 20 min. It can be seen that for a time shift of 5 min, both the correlation (0.95) and the ratio of means (0.98) stay close to 1, indicating that Taylor's hypothesis is a good approximation over short time periods. For time shifts of 10–20 min, the correlation (0.80, 0.63, 0.50) decreases rapidly. The ratio of means (0.96, 0.94, 0.91) also decreases slightly. The conclusion is that Taylor's hypothesis is not a good approximation for time shifts larger than 20 min and implies that consistent structural analysis is limited to time shifts less or equal to 20 min, corresponding to 15 km in the spatial domain.

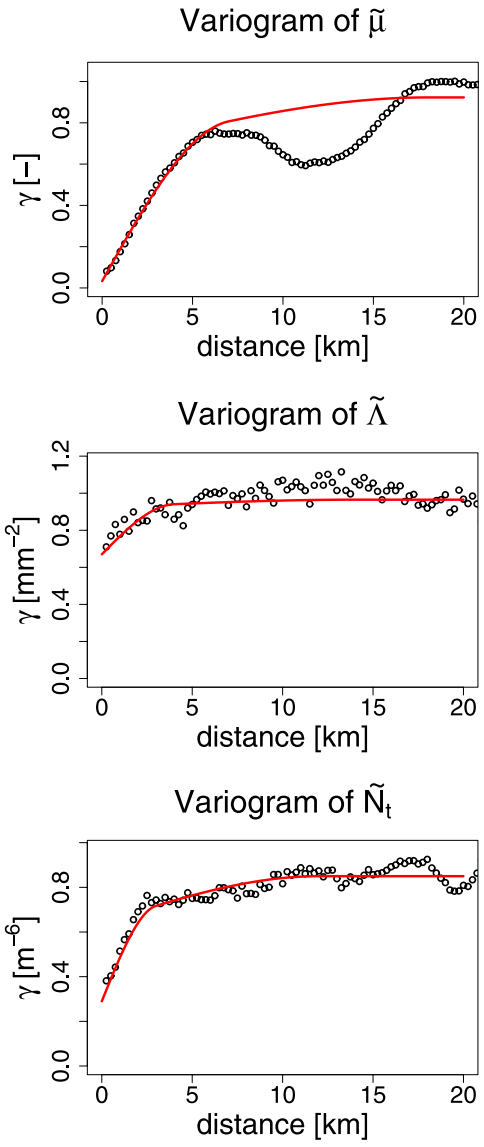

Figure 4. Sample variograms of $(\tilde{\mu}, \tilde{\Lambda}, \tilde{N}_t)$ after Gaussian anamorphosis. The values of the parameters are given in Table 1.

4.5. Fitting a Variogram Model

[28] Using Taylor's hypothesis with 12.5 m s^{-1} advection speed, the DSD time series $(\tilde{\mu}, \tilde{\Lambda}, \tilde{N}_t)$ are converted into range profiles and their sample variograms are computed. The sample variograms are fitted by combining two spherical variogram models, one for the short–range variability

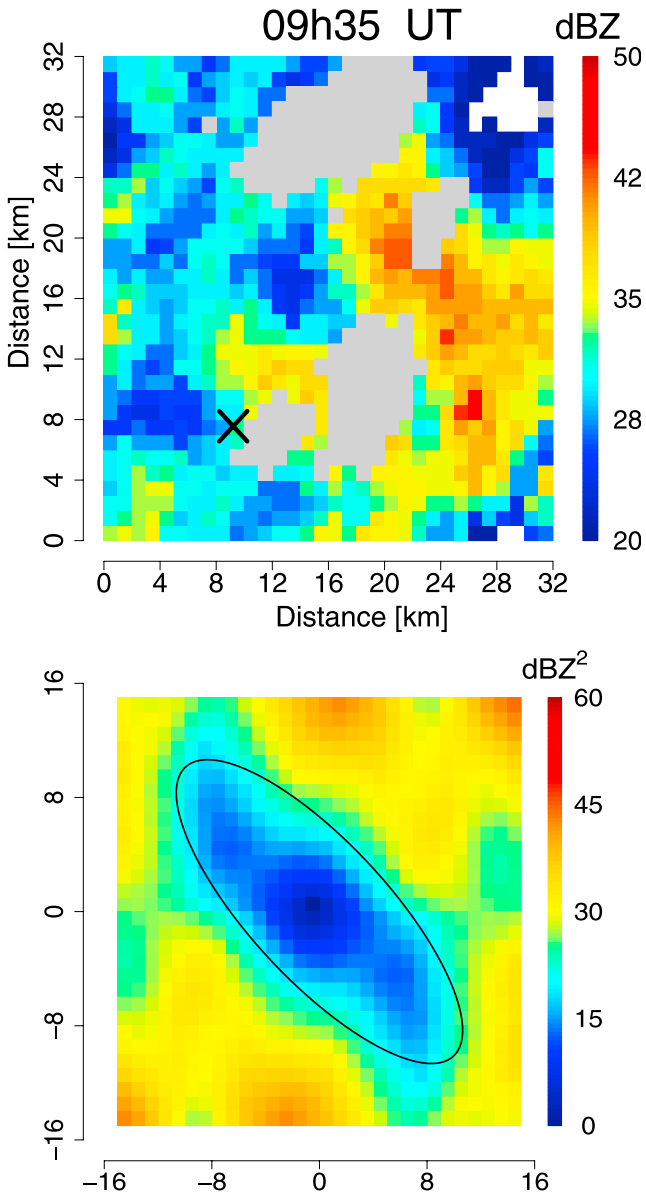

Figure 5. Observed radar reflectivity field at 0935 UT over the considered 32 × 32 km^2 domain together with its corresponding 2-D variogram map. Grey pixels correspond to ground echoes. Areas without rain are represented in white. The location of the disdrometer is indicated by the black cross in the bottom left-hand corner. The anisotropy direction is given by an azimuth of 315. The anisotropy ratio is about 0.5.

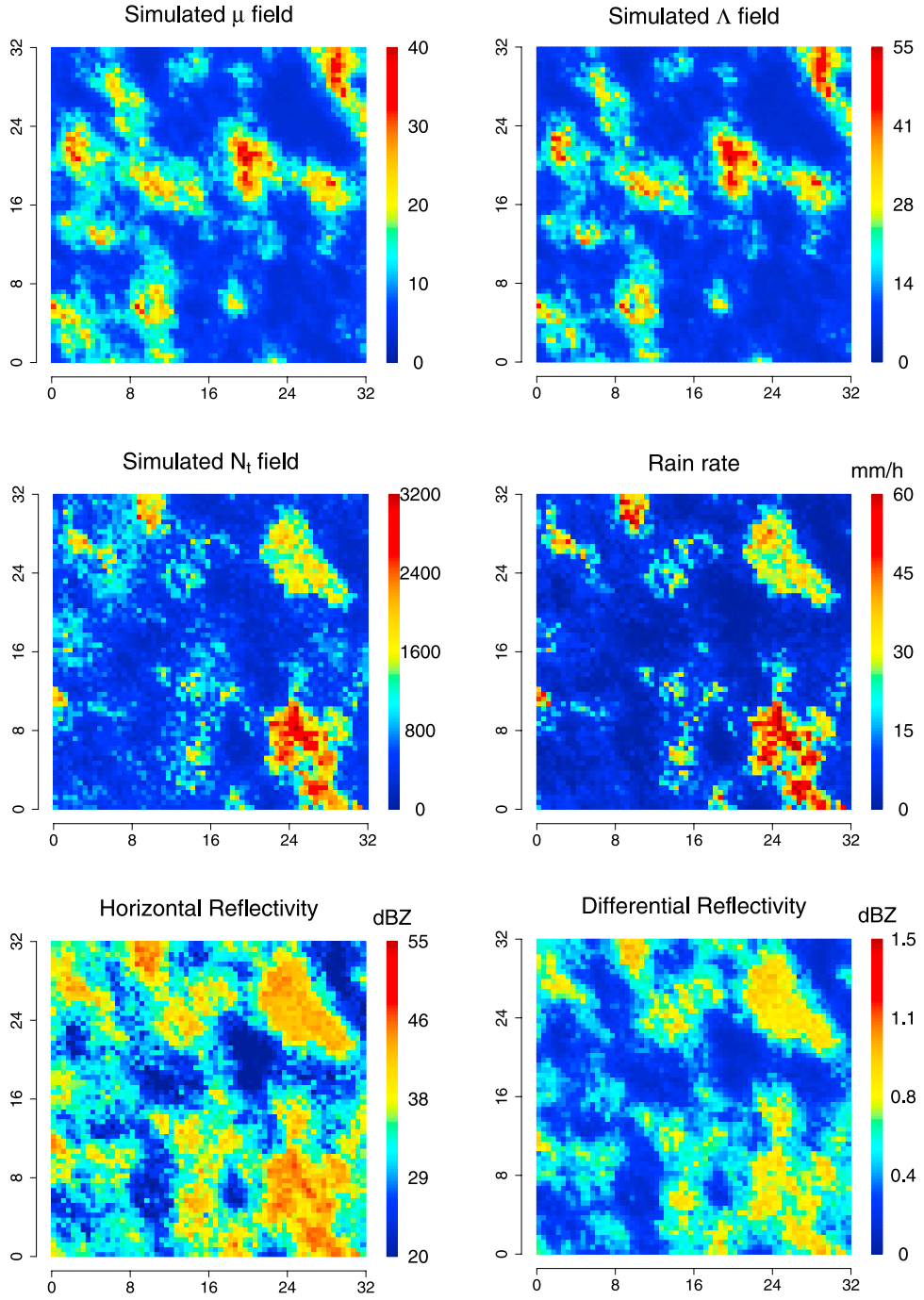

Figure 6. Example of a simulated DSD field (μ, Λ, N_t) together with its corresponding rain rate and horizontal and differential reflectivity fields.

and one for the long-range variability. A spherical variogram model is given by

$$\gamma_{sph}(h) = \begin{cases} C_0 + C_1\left(\frac{3}{2}\frac{h}{a} - \frac{1}{2}\frac{h^3}{a^3}\right) & h < a \\ C_0 + C_1 & h \geq a, \end{cases} \quad (6)$$

where C_0 denotes the nugget, C_1 the partial sill, h the interdistance and a the range. The values of the fitted parameters are given in Table 1. Figure 4 shows the fitted variograms for each DSD parameter. The total variogram for each DSD parameter is simply the sum of the two spherical models.

4.6. Estimation of the Anisotropy

[29] The variograms defined in Table 1 only describe the spatial structure along the average direction of advection. The complete two-dimensional structure of the fields can be expressed in terms of the 1-D variograms by adding information on anisotropy derived from radar reflectivity measurements. For the considered event, 28 reflectivity measurements were collected by an S band weather radar from 0835 to 1050 UT at 5-min time resolution over the

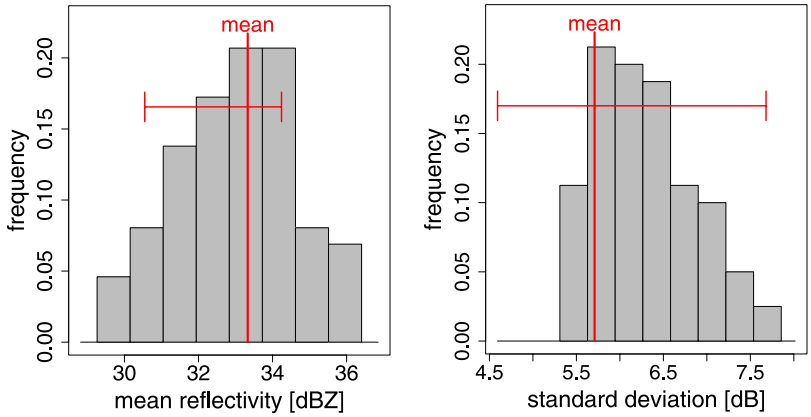

Figure 7. Histogram of the mean and of the standard deviation of 200 simulated reflectivity fields. Simulated values are represented by grey bars. The red cross represents the minimum, mean, and maximum values observed by the S band radar during the event.

considered area. The analysis of these reflectivity fields as well as their corresponding 2-D variograms indicates that the fields have geometric anisotropy (i.e., the 2-D variograms exhibit elliptic structure). The average azimuth of smallest variability (the major axis of the ellipse) is 320°. The average anisotropy ratio (the ratio between the minor and the major axis of the ellipse) is about 0.7. As an example, Figure 5 shows the radar reflectivity field and the corresponding 2-D variogram map at 0935 UT. The major axis of the anisotropy ellipse is approximatively in the NW direction (azimuth of 315°). The ratio between the minor and the major axis of the ellipse is about 0.5. In the rest of the application, the average anisotropy values (azimuth of 320° and anisotropy ratio of 0.7) are used to characterize the 2-D variograms.

4.7. Simulation of DSD Fields

[30] Using the variogram model described in Table 1 together with the average geometrical anisotropy described above, 200 Gaussian DSD fields have been simulated on a 32 × 32 km^2 domain consisting of 16′384 pixels of size 250 × 250 m^2. Such an area adequately represents the meso-γ scale and is large enough to contain all the measured variability in the DSD without being too large to avoid problems related to intermittency. Using inverse anamorphosis, the Gaussian fields are back transformed into the original DSD fields. The backscattering cross sections $\sigma_{H|V}(D)$ are computed at both horizontal and vertical polarization using the T matrix code [*Mishchenko and Travis*, 1998] and used in equation (5) to derive the corresponding reflectivity fields at S band (negligible attenuation).

[31] Figure 6 shows an example of a simulated DSD field together with the corresponding rain rate (R), horizontal reflectivity Z_h and differential reflectivity $Z_{dr} = Z_h - Z_v$ (in dB).

4.8. Comparison With Radar Measurements

[32] In order to assess the quality of the simulation, the simulated reflectivity fields Z_h derived using equation (5) are compared to the observations taken by the radar. Since the radar resolution is 1 × 1 km 2 and the simulation resolution is 250 × 250 m^2, the simulations are averaged over blocks of 4 × 4 pixels before comparison. Moreover, all ground echoes have been removed from the data before the comparison. To avoid issues due to intermittency, the comparison is restricted to radar measurements taken from 0915 to 0955 UT (10 measurements), for which intermittency is negligible. The selected fields have mean values ranging from 30.5 to 34.2 dBZ, with an average of 33.8 dBZ. The standard deviation of the observed fields is between 4.6 dBZ and 7.6 dBZ, with an average of 5.6 dBZ. Figure 7 shows that these values are in good agreement with the simulated fields. Indeed, the simulated reflectivity fields have mean values between 29.3 dBZ and 36.4 dBZ, with an average of 32.9 dBZ and their standard deviations are between 5.3 dBZ and 7.9 dBZ, with an average of 6.3 dBZ. This shows that the simulated fields adequately reproduce the first-order moments (mean and standard deviation) of the observed reflectivity fields. Furthermore, the simulations also exhibit a similar asymmetry in the distributions as shown in Figure 7.

[33] Figure 8 shows a comparison between the spatial structure of the simulations and the spatial structure of the observations. In order to keep Figure 8 readable, an average

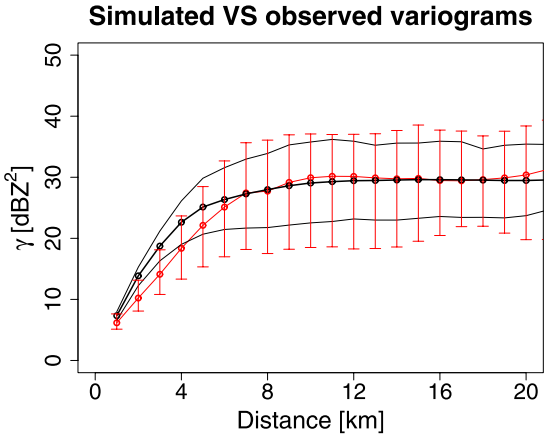

Figure 8. Average radar reflectivity variogram (in red with vertical bars) and average simulated reflectivity variogram (in black). The lower and upper bounds represent the 10% and 90% variogram quantiles for each distance class computed on 28 radar pictures and 200 simulations.

variogram has been plotted for both simulated and observed reflectivity fields. The dispersion about the average variogram is represented (for each distance class) by the 10% and 90% quantiles. It can be seen that the simulated and observed variograms are in good agreement except for the first 2–3 km where the simulations exhibit slightly too much variability. Different explanations can be given for this. (1) There is a smoothing effect in the observed reflectivity fields due to the power distribution in the radar beam. Hence, radar pixels that are far away from the antenna are averaged over large overlapping volumes and exhibit more correlation. This implies a smaller slope in the variograms computed using radar observations, especially at small interdistances where the averaging effect is the strongest. (2) The Gaussian anamorphosis described in section 2.2 was computed on a small sample of 415 DSD observations. The inverse transformation was approximated using a correspondence table between the original and transformed variables. The discretization introduced by this technique may explain the rather strong variability at short ranges in the simulations. (3) Taylor's hypothesis of frozen turbulence was shown to be acceptable but not perfect. Furthermore, parameters like the advection speed, the anisotropy direction and anisotropy ratio were estimated using radar data and supposed constant over the entire event, which is not exactly true.

[34] Despite the above mentioned problems, the proposed simulator produces very encouraging results that are consistent with the observations. The simulated 2-D fields are in good agreement in terms of first- and second-order moments. The spatial structure is also in good agreement with the observations.

5. Conclusions

[35] DSD fields are highly variable in space and time. To investigate issues related to this variability in radar rain rate estimation, a stochastic simulation framework has been proposed in the present paper. It is based on a geostatistical approach that considers the Gamma DSD parameters (μ, Λ, N_t) as realizations of a multivariate random function.

[36] To take advantage of simple and fast Gaussian field simulation algorithms, the distribution of the three DSD parameters is normalized using a Gaussian anamorphosis technique. The spatial structure of the fields is quantified using variograms. Gaussian fields with identical spatial structure are generated and back transformed into the original distributions. In this way, realistic conditional or nonconditional 2-D fields of DSDs can be generated.

[37] The proposed approach is applied to DSD measurements collected during an intense Mediterranean rainfall event. As only DSD time series are available, Taylor's hypothesis is invoked to convert time series into range profiles. The anisotropy direction and anisotropy ratio of the fields are derived from measurements taken by an S band weather radar. Reflectivity fields derived from the simulations are compared to radar measurements. Both the mean and the standard deviation are in very good agreement. The spatial structure is also coherent with the observations, indicating that the proposed simulator can reproduce realistic 2-D fields of DSDs.

[38] The main limitation of the proposed simulator is its inability to simulate intermittent DSD fields. This limits the size of the simulated domains to the meso-γ scale (about 20 km) at which nonintermittent rain fields are plausible. Taylor's hypothesis is not required to run the simulator, but is used because of the lack of spatial DSD measurements. Better results can even be expected when spatial DSD data will be available. Future work will mainly focus on the intermittency problem and on alternatives to the anamorphosis technique.

[39] **Acknowledgments.** The first two authors acknowledge the financial support from the Swiss National Science Foundation (grant 200021-118057/1). The last author acknowledges the financial support of the EC project HYDRATE-Hydrometeorological Data Resources and Technologies for Effective Flash Flood Forecasting (GOCE-037024).

References

Andsager, K., K. V. Beard, and N. F. Laird (1999), Laboratory measurements of axis ratios for large rain drops, *J. Atmos. Sci.*, *56*(15), 2673–2683.

Beard, K. V. (1976), Terminal velocity and shape of cloud and precipitation drops aloft, *J. Atmos. Sci.*, *33*(5), 851–864.

Berndtsson, R., and J. Niemczynowicz (1988), Spatial and temporal scales in rainfall analysis, some aspects and future perspectives, *J. Hydrol.*, *100*(1-4), 293–313.

Berne, A., and R. Uijlenhoet (2005), A stochastic model of range profiles of raindrop size distributions: Application to radar attenuation correction, *Geophys. Res. Lett.*, *32*, L10803, doi:10.1029/2004GL021899.

Berne, A., G. Delrieu, J.-D. Creutin, and C. Obled (2004), Temporal and spatial resolution of rainfall measurements required for urban hydrology, *J. Hydrol.*, *299*(3-4), 166–179.

Bouvier, C., L. Cisneros, R. Dominguez, J.-P. Laborde, and T. Lebel (2003), Generating rainfall fields using principal components (PC) decomposition of the covariance matrix: a case study in Mexico City, *J. Hydrol.*, *278*(1-4), 107–120.

Chilés, J.-P., and P. Delfiner (1999), *Geostatistics: Modeling Spatial Uncertainty*, 695 pp., John Wiley, New York.

Cressie, N., and D. M. Hawkins (1990), Robust estimation of the variogram, *J. Math. Geol.*, *12*(2), 115–125.

Dicicciо, T., M. Martin, and G. Young (1993), Analytical approximations to conditional distribution functions, *Biometrika*, *80*(4), 781–790.

Dissanayake, A., J. Allnutt, and F. Haidara (1997), A prediction model that combines rain attenuation and other propagation impairments along Earth-satellite paths, *IEEE Trans. Antennas Propag.*, *45*(10), 1546–1558, doi:10.1109/8.633864.

Fong, B., P. B. Rapajic, G. Y. Hong, and A. C. M. Fong (2003), Factors causing uncertainties in outdoor wireless wearable communications, *IEEE Pervasive Comput.*, *2*(2), 16–19, doi:10.1109/MPRV.2003.1203748.

Foufoula-Georgiou, E., and W. F. Krajewski (1995), Recent advances in rainfall modeling, estimation, and forecasting, *Rev. Geophys.*, *33*(S1), 1125–1137.

Groisman, P. Y., and D. R. Easterling (1994), Variability and trends of total precipitation and snowfall over the United States and Canada, *J. Clim.*, *7*(1), 184–205.

Guillot, G. (1999), Approximation of Sahelian rainfall fields with meta-Gaussian random functions—Part 1: Model definition and methodology, *Stochastic Environ. Res. Risk Assess.*, *13*(1-2), 100–112.

Gupta, V. K., and E. Waymire (1993), A statistical analysis of mesoscale rainfall as a random cascade, *J. Appl. Meteorol.*, *32*(2), 251–267.

Haddad, Z. S., D. A. Short, S. L. Durden, E. Im, S. Hensley, M. B. Grable, and R. A. Black (1997), A new parametrization of the rain drop size distribution, *IEEE Trans. Geosci. Remote Sens.*, *35*(3), 532–539.

Hall, P., R. Wolff, and Q. Yao (1999), Methods for estimating a conditional distribution function, *J. Am. Stat. Assoc.*, *94*, 154–163.

Jameson, A. R., and A. B. Kostinski (2001), What is a raindrop size distribution?, *Bull. Am. Meteorol. Soc.*, *82*(6), 1169–1177.

Journel, A. G., and C. J. Huijbregts (1978), *Mining Geostatistics*, 600 pp., Academic, London.

Kliche, D., P. Smith, and R. Johnson (2008), L-moment estimators as applied to gamma drop size distributions, *J. Appl. Meteorol. Climatol.*, *47*, 3117–3130, doi:10.1175/2008JAMC1936.1.

Krajewski, W. F., R. Raghavan, and V. Chandrasekar (1993), Physically based simulation of radar rainfall data using a space-time rainfall model, *J. Appl. Meteorol.*, *32*(2), 268–283.

Lantuéjoul, C. (2002), *Geostatistical Simulation, Models and Algorithms*, 256 pp., Springer, Berlin.

Lavergnat, J., and P. Golé (2006), A stochastic model of raindrop release: Application to the simulation of point rain observations, *J. Hydrol.*, *328*(1–2), 8–19.

Lee, G., A. W. Seed, and I. Zawadzki (2007), Modeling the variability of drop size distributions in space and time, *J. Appl. Meteorol. Climatatol.*, *46*(7), 742–756, doi:10.1175/JAM2505.1.

Leuangthong, O., and C. V. Deutsch (2003), Stepwise conditional transformation for simulation of multiple variables, *Math. Geol.*, *35*(2), 155–173.

Mardia, K. (1970), Measures of multivariate skewness and kurtosis with applications, *Biometrika*, *57*, 519–530.

Matheron, G. (1965), *Les Variables Régionalisées et Leur Estimation*, 305 pp., Masson et Cie, Paris.

Menabde, M., A. Seed, D. Harris, and G. Austin (1997), Self-similar random fields and rainfall simulation, *J. Geophys. Res.*, *102*(D12), 13,509–13,515.

Mishchenko, M. I., and L. D. Travis (1998), Capabilities and limitations of a current FORTRAN implementation of the T-matrix method for randomly oriented, rotationally symmetric scatterers, *J. Quant. Spectrosc. Radiat. Transfer*, *60*(3), 309–324.

Montopoli, M., F. S. Marzano, and G. Vulpiani (2008), Analysis and synthesis of raindrop size distribution time series from disdrometer data, *IEEE Trans. Geosci. Remote Sens.*, *46*(2), 466–478, doi:10.1109/TGRS.2007.909102.

Onof, C., R. E. Chandler, A. Kakou, P. Northrop, H. S. Wheater, and V. Isham (2000), Rainfall modelling using Poisson-cluster processes: A review of developments, *Stochastic Envron. Res. Risk Assess.*, *14*(6), 384–411.

Orlanski, I. (1975), A rational subdivision of scales for atmospheric processes, *Bull. Am. Meteorol. Soc.*, *56*(5), 527–530.

Pebesma, E. J. (2004), Multivariate geostatistics in S: The Gstat package, *Comput. Geosci.*, *30*(7), 683–691, doi:10.1016/j.cageo.2004.03.012.

Pegram, G. G. S., and A. N. Clothier (2001), High resolution space-time modelling of rainfall: The "string of beads" model, *J. Hydrol.*, *241*(1–2), 26–41.

Srivastava, M., and T. Hui (1987), On assessing multivariate normality based on Shapiro-Wilk W statistic, *Stat. Probab. Lett.*, *5*, 15–18.

Syed, T. H., V. Lakshmi, E. Paleologos, D. Lohmann, K. Mitchell, and J. S. Famiglietti (2004), Analysis of process controls in land surface hydrological cycle over the continental United States, *J. Geophys. Res.*, *109*, D22105, doi:10.1029/2004JD004640.

Tokay, A., and D. A. Short (1996), Evidence from tropical raindrop spectra of the origin of rain from stratiform versus convective clouds, *J. Appl. Meteorol.*, *35*(3), 355–371.

Uijlenhoet, R., M. Steiner, and J. A. Smith (2003), Variability of raindrop size distributions in a squall line and implications for radar rainfall estimation, *J. Hydrometeorol.*, *44*(4), 43–61.

Uijlenhoet, R., J. M. Porrà, D. Sempere Torres, and J.-D. Creutin (2006), Analytical solutions to sampling effects in drop size distribution measurements during stationary rainfall: Estimation of bulk rainfall variables, *J. Hydrol.*, *328*(1), 65–82, doi:10.1016/j.jhydrol.2005.11.043.

Ulbrich, C. W. (1983), Natural variations in the analytical form of the raindrop-size distribution, *J. Clim. Appl. Meteorol.*, *22*(10), 1764–1775.

Ulbrich, C. W., and D. Atlas (1998), Rainfall microphysics and radar properties: analysis methods for drop size spectra, *J. Appl. Meteorol.*, *37*(9), 912–923.

van der Vaart, A. W. (1998), *Asymptotic Statistics*, 443 pp., Cambridge Univ. Press, Cambridge, U. K.

Waymire, E., V. K. Gupta, and I. Rodriguez-Iturbe (1984), A spectral theory of rainfall intensity at the meso-β scale, *Water Resour. Res.*, *20*(10), 1453–1465.

Willis, P. T. (1984), Functional fits to some observed drop size distributions and parameterization of rain, *J. Atmos. Sci.*, *41*(9), 1648–1661.

Xie, P., and P. A. Arkin (1997), Global precipitation: A 17-year monthly analysis based on gauge observations, satellite estimates and numerical model outputs, *Bull. Am. Meteorol. Soc.*, *78*(11), 2539–2558.

Xue, M., K. K. Droegemeier, and V. Wong (2000), The Advanced Regional Prediction System (ARPS)—A multi-scale nonhydrostatic atmospheric simulation and prediction model. Part I: Model dynamics and verification, *Meteorol. Atmos. Phys.*, *75*(3–4), 161–193, doi:10.1007/s007030070003.

Yaglom, A. (2004), *An Introduction to the Theory of Stationary Random Functions*, 256 pp., Dover, Mineola, N. Y.

A. Berne and M. A. Schleiss, Laboratoire de Télédétection Environnementale, École Polytechnique Fédérale de Lausanne, CH-1015 Lausanne, Switzerland. (alexis.berne@epfl.ch; marc.schleiss@epfl.ch)

R. Uijlenhoet, Hydrology and Quantitative Water Management, Wageningen University, NL-6700 HB Wageningen, Netherlands. (eemko.uijlenhoet@wur.nl)